Model predictive control of voltage profiles in MV networks with distributed generation

M. Farina [a,*], A. Guagliardi [b], F. Mariani [a,1], C. Sandroni [b], R. Scattolini [a]

[a] *Dipartimento di Elettronica, Informazione e Bioingegneria, Politecnico di Milano, Via Ponzio 34/5, Milano, Italy*
[b] *RSE, Via Rubattino 54, Milano, Italy*

1. Introduction

The ever increasing diffusion of renewable distributed generators (DG) raises new technological problems in the management and control of Medium Voltage (MV) and Low Voltage (LV) distribution networks. In fact, distributed generators can induce local voltage increase, with inversion of power flows and emergence of inverse currents along the feeders of radial networks, so that voltage control is becoming of paramount importance for making further progress of the field possible. At the same time, the improved information and communication capabilities of modern Smart Grids (SG) allow to develop innovative control schemes and procedures which have to be fully exploited to guarantee a sustainable growth of distributed generation.

In recent years many solutions have been proposed to the voltage control problem, based on coordinated or uncoordinated schemes, see e.g. (Kiprakis & Wallace, 2003; Vovos, Kiprakis, Wallace, & Harrison 2007; Viawan & Karlsson, 2008; Xu & Taylor, 2008; Hojo, Hatano, & Fuwa 2009; Gao & Redfern, 2010; Aquino-Lugo, Klump, & Overbye 2011; Turitsyn, Šulc, Backhaus, & Chertkov 2011; Yu, Czarkowski, & de Leon 2012; Liu, Aichhorn, Liu, & Li 2012). In coordinated solutions, a centralized controller maintains prescribed voltage profiles and reactive power flows, see e.g. Vovos et al. (2007), (Viawan & Karlsson, 2008), usually acting on an On-Load Tap Changer (OLTC) transformer, (see Gao & Redfern, 2010), or on additional Energy Storage Systems (ESS) used to reduce the OLTC operations, (see Liu et al., 2012). In uncoordinated schemes, the voltage and reactive power control equipments spread over the network are allowed to locally regulate the terminal bus voltage by adjusting their reactive power output (see Vovos et al., 2007). Both coordinated and uncoordinated schemes have their own advantages and drawbacks. Coordinated control structures are potentially less reliable and prone to communication losses, local faults and overall vulnerability but, on the contrary, they usually rely on the solution of a global Optimal Power Flow (OPF) problem, as such they can reduce losses and optimize the voltage and reactive power profiles. Concerning uncoordinated solutions, they may display serious technical

* Corresponding author. Tel.: +39 02 2399 3599.
  E-mail addresses: marcello.farina@polimi.it (M. Farina),
guagliardi@rse-web.it (A. Guagliardi), marianifederico@gmail.com (F. Mariani),
sandroni@rse-web.it (C. Sandroni), riccardo.scattolini@polimi.it (R. Scattolini).

[1] F. Mariani has been Ms student at the Politecnico di Milano.

drawbacks, see again (Vovos et al., 2007), (Turitsyn et al., 2011). However, the flexibility provided for example by photovoltaic generators with inverters, together with their wider and wider diffusion, will inevitably lead to their massive participation in voltage control in the future.

A fundamental problem in the design of dynamic controllers, both for coordinated and for uncoordinated schemes, is due to the difficulty to obtain reliable, yet possibly simple, dynamic models of the system, due to the potentially large number of elements of the network (generators and loads), and to the intrinsic complexity of the system. For this reason, most of the above cited solutions rely on models derived under the assumption that the network is in a permanent periodic regime, or obtained by means of a sensitivity analysis, see with (Richardot, Viciu, Besanger, & Kieny 2006), (Biserica, Bersaneff, Besanger, & Kieny 2011), (Valverde & Van Cutsem, 2013). This prevents one from using classical dynamic control techniques, and the transient performance of the controlled system subject to disturbances are neglected, such as the transient response in front of varying loads or power production of the DGs.

For these reasons, in this paper a new dynamic model-based approach for voltage control in MV networks is proposed and applied. First, a dynamic MIMO impulse response model of the network is obtained with simple experiments on a realistic and reliable industrial simulator (hence making this procedure general and applicable to experimental test beds, since similar models can be obtained with non-invasive experiments on real systems). Then, an overall control system, organized according to a hier-archical (cascade) thee-layer structure, is proposed, as suggested among the others in (Xu & Taylor, 2008). At the upper level, a static OPF problem is solved and the voltage and reactive power references at the nodes of the grid are computed. Based on the OPF solution, at the intermediate level a centralized controller computes the reference values for the local power factors of the distributed generators. Finally, at the lower level, these reference power factors are transformed into reference values of reactive power and local Automatic Voltage Regulators (AVR) are designed, one for each DG participating in the control action. Since the upper and the lower levels are quite standard, in the paper focus is placed on the design of the centralized controller at the inter-mediate level. This controller is designed with a Model Predictive Control (MPC) algorithm (Camacho & Bordons, 2007), in view of its capability to explicitly handle constraints on the main process variables, such as the voltages along the grid or the adopted power factors. In addition, by including suitable slack variables in the optimization problem underlying the MPC formulation, possible infeasibility conditions can be detected, due for example to excessive load or generated power variations. In these cases, the tap changer position is modified to recover feasibility and to maintain the voltages inside the prescribed band.

The considered case study consists of a rural MV [20 kV] radial network, located in the center of Italy, with two feeders, eight distributed generators and thirty-one loads, whose characteristics are reported in the Appendix A. A detailed simulator of the network has been first developed in the DIgSILENT PowerFactory® environment and has been used to obtain the impulse response representation of the system. Then, the MPC algorithm has been implemented in the MATLAB environment and has been tested on the DIgSILENT simulator by considering four significantly different scenarios, corresponding to different hours of the day, so as to consider a highly realistic test case.

The paper is organized as follows. In Section 2 the overall control structure is described and the MPC algorithm is intro-duced. Section 3 is devoted to present a number of simulation results and compares the performances of the proposed method with those provided by a classic PI-based centralized control scheme. Finally, some conclusions and hints for future research are reported in Section 4.

2. Methodology: control structure and MPC design

The proposed control structure is made by three layers; at the upper layer (tertiary control) a static OPF is periodically solved and the optimal voltage profiles along the distribution network are computed based on the current status of the network and on the prediction of the future loads and active power production. At the intermediate layer (secondary control), a centralized MPC regulator
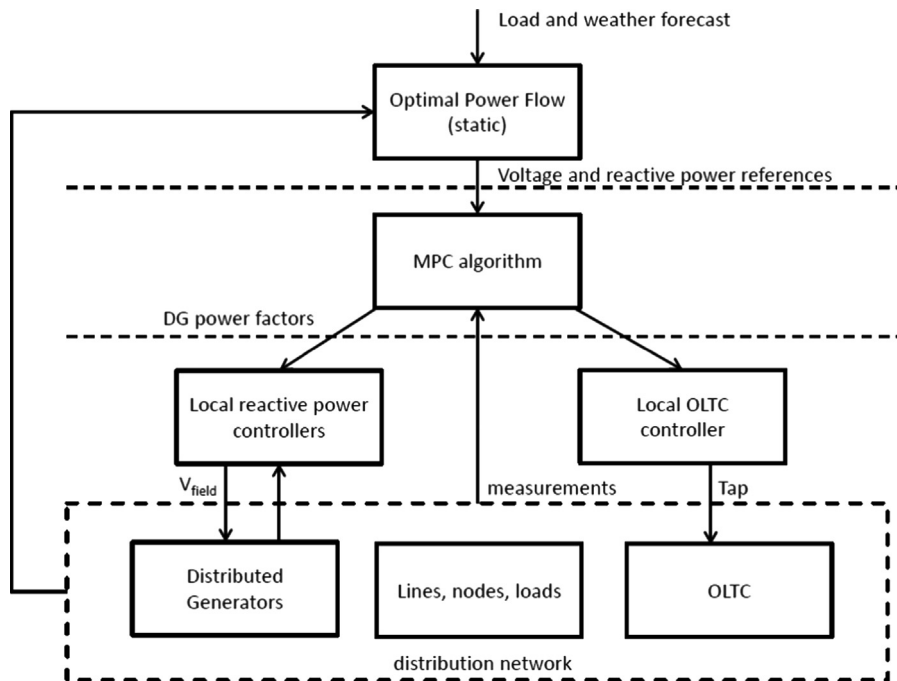

Fig. 1. The hierarchical control structure.

computes the reference power factors for the DGs participating in voltage control, based on the solution of the OPF and on the available voltage measurements. At the lower layer (primary con-trol), the reference power factors are transformed in reactive power references and local AVRs are used to control the reactive powers by acting on the excitation voltages of the DGs. A schematic represen-tation of the control structure is shown in Fig. 1.

In the following, focus is placed on the design of the centralized controller at the intermediate layer. In fact, well established techniques and tools are already available for OPF, see e.g. Huneault and Galiana (1991). Moreover, the synthesis of the local AVR regulators, usually PI-PID, is in general not critical due to the satisfactory frequency decoupling of these control loops, see e.g. Petrone et al. (2012) where some preliminary results of this research have been reported.
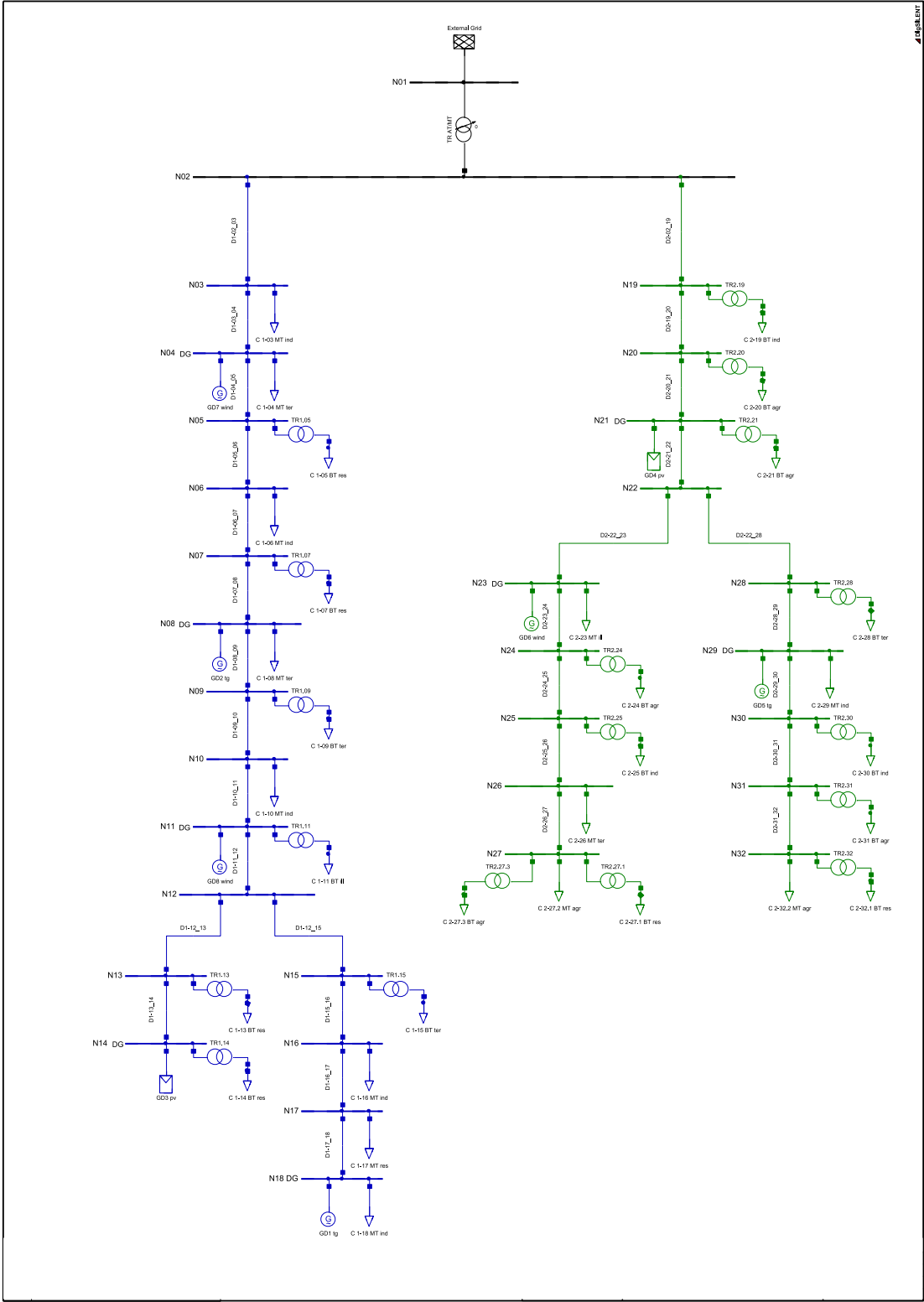

Fig. 2. The benchmark network.

2.1. Input–output dynamic model of the network

In the design phase we will use impulse response models of the network, including the AVR control loops, which can be obtained by means of simple experiments on the real system or on a detailed dynamic simulator, such as the one developed in this work with DIgSILENT PowerFactory®, a powerful and widely used industrial simulation environment. One of the main advantages of relying on input–output models, like the impulse response models used here, is that state estimators are not required. This is fundamental, in this framework, due to the presence of a large number of unknown and time-varying disturbances (usually larger than the number of measured variables), such as loads or produced power. It is also worth noting that, despite their simplicity, these models are capable of robustly and reliably capturing the main dynamics of the network, differently from the static and/or sensitivity-based models used, e.g., in Valverde and Van Cutsem (2013).

Consistently, we adopt the following truncated linear discrete-time impulse representation of the system

$$y(k) = \sum_{i=1}^{M} \left[g_i u(k-i) + \gamma_i d(k-i) \right] + \delta(k)$$

where k is the discrete time index, y is the vector of the controlled variables (deviations of the voltages with respect to their nominal values at specified nodes of the grid), u is the vector of the control variables (deviations of the power factor references), d is the vector

Table 1
Step variations of DGs and in the open loop simulation for identification. DGi_P and DGi_Q denote the active and reactive, respectively, power of the distributed generator DGi.

Input variable	Step amplitude
DG1_Q	2.3750000 [MVAR]
DG2_Q	1.3880000 [MVAR]
DG3_Q	0.7650000 [MVAR]
DG4_Q	0.7600000 [MVAR]
DG5_Q	2.3850000 [MVAR]
DG6_Q	0.2660000 [MVAR]
DG7_Q	0.2660000 [MVAR]
DG8_Q	0.2660000 [MVAR]
DG1_P	−0.9845622 [MW]
DG2_P	−0.5728366 [MW]
DG3_P	0.3118806 [MW]
DG4_P	0.3118806 [MW]
DG5_P	−0.9845612 [MW]
DG6_P	0.16475837 [MW]
DG7_P	0.16475837 [MW]
DG8_P	0.16475837 [MW]

of measurable disturbances (possible known deviations of the active and the reactive power of the loads), δ is an additional unknown term summarizing the contribution of all the unknown exogenous signals (deviations of the unmeasurable loads) acting on the system, and g_i, γ_i are the impulse response coefficients. In view of the stability properties of the system, it is assumed that the impulse response is practically exhausted after M sampling times.

The variable δ is introduced to account for unmodelled dynamics, perturbed operating conditions, possible disturbances, and unmeasurable exogenous signals. Consistently with classic solutions adopted in the MPC control framework, see e.g., (Camacho & Bordons, 2007), an estimate of δ can be obtained by computing, at time step k, the following value

$$\hat{\delta}(k) = y(k) - \sum_{i=1}^{M} g_i u(k-i) + \gamma_i d(k-i)$$

and assuming that it will remain constant over the future prediction horizon.

Details on the application of the described identification technique to the case study can be found in Section 3.2.

2.2. The MPC-based algorithm

The centralized controller at the intermediate layer is designed with MPC, a very popular method in the process industry which relies on the recursive solution of a constrained optimization problem, see (Camacho & Bordons, 2007). The MPC approach has been selected for the following reasons:

- Hard constraints can be easily included in the optimization problem to be solved on-line at any sampling time for the computation of the main control variables, i.e., the reference power factors of the DGs. This is a fundamental point, since in practical applications the zero-error asymptotic tracking of the voltage reference values at prescribed points of the grid is not the main issue. On the contrary, it must be guaranteed that these voltages remain inside the statutory limits, that reverse power flows are avoided, and that the operational constraints on the adopted power factors are fulfilled. Note that, this is not *a priori* guaranteed by baseline methods currently applied on networks.
- Voltage deviations at specified nodes of the network can be differently weighted in the performance index to be recursively minimized, so that flexibility is easily achieved in the control problem formulation.
- Future predicted variations of the loads and of the power produced by some DGs (such as PVs) can be accounted for to enhance the control performance.
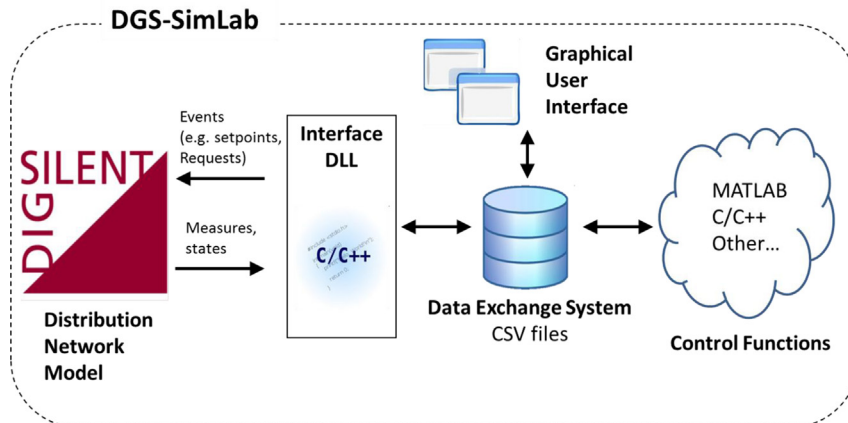

Fig. 3. DGS-SimLab interface between the control scheme and the reference simulator.

Using the impulse response model devised in Section 2.1 and assuming that the disturbance δ remains constant over the future prediction horizon (of length N), the i steps-ahead prediction $y(k+i)$, computed at time k, can be given the form

$$y(k+i) = \sum_{j=1}^{i} (g_j u(k+i-j) + \gamma_j d(k+i-j)) + y(k)$$
$$+ \sum_{j=i+1}^{M} (g_j u(k+i-j) + \gamma_j d(k+i-j))$$
$$- \sum_{j=1}^{M} (g_j u(k-j) + \gamma_j d(k-j))$$

this prediction is a function of the past, present and future control actions and of the current output and it is used in the constrained optimization problem stated below. Denoting with N and N_u the prediction horizon and the control horizon, respectively, with $N_u \leq N$, and defining

$$Y = \begin{bmatrix} y(k+1) \\ y(k+2) \\ \vdots \\ y(k+N) \end{bmatrix}, \quad U = \begin{bmatrix} u(k) \\ u(k+1) \\ \vdots \\ u(k+N_u-1) \end{bmatrix}$$

the MPC optimization problem is

$$\min_{U, \varepsilon_1, \varepsilon_2} Y'QY + U'RU + \mu_1 \varepsilon_1^2 + \mu_2 \varepsilon_2^2$$

subject to the following constraints on the input and output variables

$$U_{min} \leq U \leq U_{max}$$
$$-\varepsilon_1 \mathbf{1} + Y_{min} \leq Y \leq \varepsilon_2 \mathbf{1} + Y_{max}$$
$$\varepsilon_1 \geq 0, \quad \varepsilon_2 \geq 0$$

Table 2
Power variations of DGs and loads in Experiment 1.

Node	Time	Variation
N32-2	20 s	50% increase of the load active and reactive power with respect to nominal values
DG2	100 s	Active power step variation with final value 1.75 [MW]
N08	150 s	100% increase of the load active and reactive power with respect to nominal values
DG5	200 s	Active power step variation with final value 3.75 [MW]
N16	300 s	50% reduction of the load active and reactive power with respect to nominal values
DG8	600 s	Active power step variation with final value 3 [MW]

The matrices Q and R are positive definite and symmetric, $\mu_1 > 0$, $\mu_2 > 0$, and the prediction horizon N must be selected to include the main system's dynamics. The control horizon N_u is used in MPC to allow for only a limited number of variations of the future control variables, i.e. in the optimiziation problem it is set $u(k+N_u+i) = u(k+N_u-1)$, $i > 0$. The terms U_{min}, U_{max}, Y_{min}, Y_{max} represent physical bounds on the control and controlled variables (recall that variables $u(k)$ and $y(k)$ denote deviations with respect to nominal values), $\mathbf{1}$ is a vector of elements equal to one, and ε_1, ε_2 are *slack variables*, introduced to allow soft constraints on the outputs, so as to guarantee feasibility also when disturbances (loads or generators variations) suddenly move the network away from its nominal operating conditions. This general formulation is very flexible, since additional constraints on the control variations at any sampling time, or on the maximum deviation allowed between two output (voltages) at adjacent nodes of the network, can be easily included to adapt the optimization problem to any specific requirement in terms of performance and constraints. As already noted, in the voltage control problem, these constraints have the highest importance, while the requirement of exact tracking of voltage reference values is less relevant. For this reason, no integral action has been included in the regulator structure.
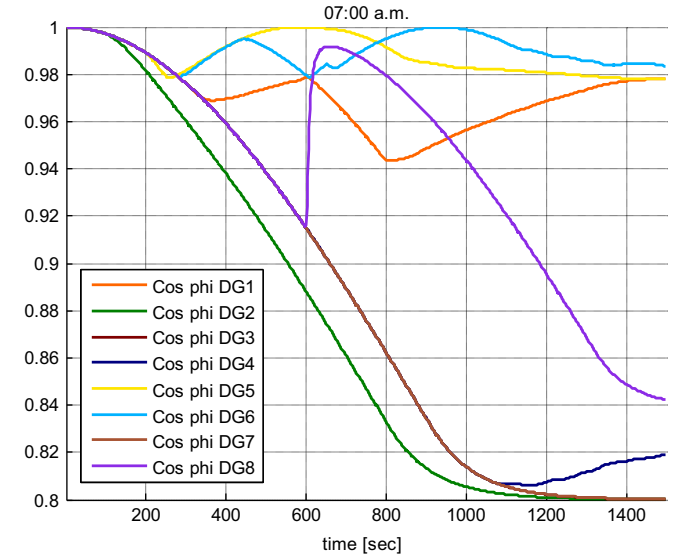
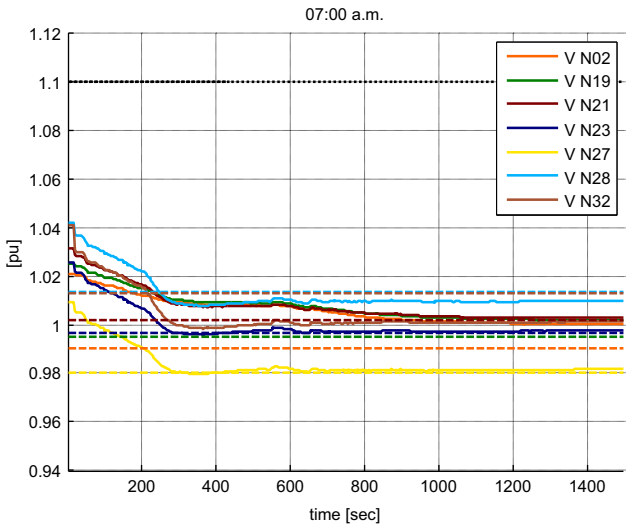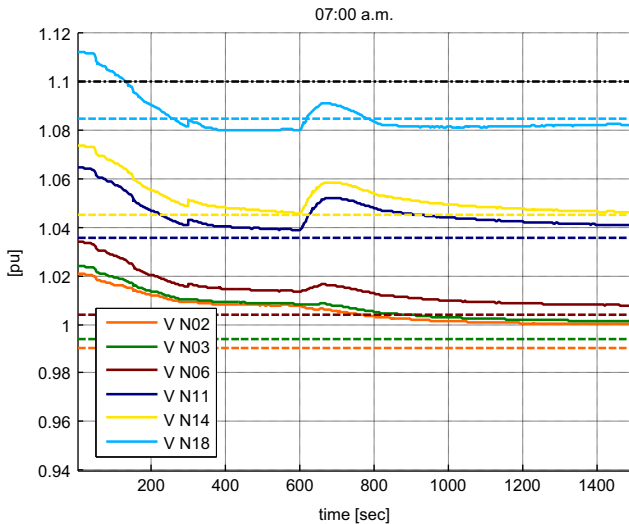**Fig. 5.** Experiment 1–7 a.m. reference power factors computed by the MPC algorithm.

Fig. 4. Experiment 1–7 a.m. voltages at the nodes of the first (left) and second (right) feeder. Dashed lines: reference values. Dash-dotted black line: $1+Y_{max}$.

Fig. 6. Experiment 1–1 p.m. voltages at the nodes of the first (left) and second (right) feeder. Dashed lines: reference values. Dash-dotted black line: $1 + Y_{max}$.

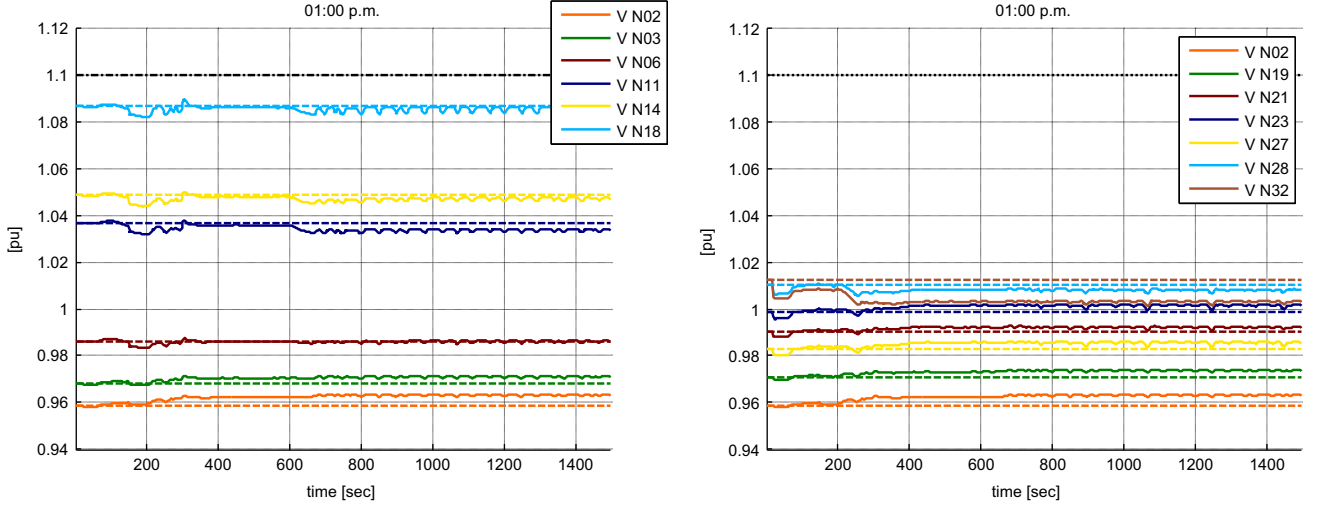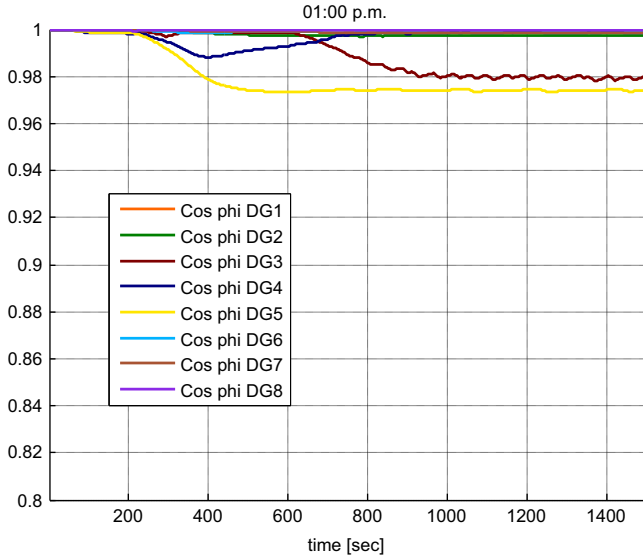

Fig. 7. Experiment 1–1 p.m. reference power factors computed by the MPC algorithm.

The above optimization problem is QP (Quadratic Program), and can be efficiently solved at any time instant to compute the optimal sequence $u(k)$, ..., $u(k+N_u-1)$ of future control variables. Then, according to the so-called Receding Horizon principle, only the first value $u(k)$ of this sequence is effectively applied and the overall procedure is repeated at the next sampling time.

2.2.1. Remark

The proposed MPC algorithm does not guarantee *a priori* the closed-loop stability. This could seem to be unnecessarily limitative, since many MPC algorithms with stabilizing properties have been developed, see (Mayne, Rawlings, Rao, & Scokaert 2000), by including in the optimization problem suitable terminal cost and/ or terminal constraints. To this regard, two comments are in order. First, the adopted impulse response model is largely overparametrized, which indeed is the price to be paid for the use of such a simple empirical modeling procedure. In turn, this overparametrization would imply a very high computational effort in the design of the stabilizing parameters, i.e. the terminal cost and the terminal constraint. Second, the schemes most commonly used in industrial practice are characterized by the use of sufficiently long prediction horizons, which implicitly lead to closed-loop stability, as well assessed by many theoretical results nowadays available for unconstrained MPC, see (Jadbabaie & Hauser), (Grüne & Rantzer).

2.3. The OLTC controller

Large variations of the active power produced by the DG's and/ or of the network loads can lead to the impossibility to maintain the voltages along the grid within the nominal operation bound (corresponding to the constraint $Y_{min} \leq Y \leq Y_{max}$ as far as the deviation variable $y(t)$ is concerned) by solely modifying the DG's power factors using the MPC algorithm previously described. For a prompt response to this undesired situation, the regulation scheme activates the OLTC when violations are revealed. Constraints violations are detected when the slack variables included into the optimization problem to guarantee feasibility (i.e., $\varepsilon_1,\ \varepsilon_2$) take strictly positive values. For this reason, the OLTC control is activated by the slack variables. Specifically, letting $\delta\varepsilon = \varepsilon_2 - \varepsilon_1$, three cases can occur and the proper control actions can be taken:

- $\delta\varepsilon = 0$ if the upper and lower constraints on the voltages along the feeders are satisfied or if they are violated with equal values ε_1 and ε_2. In both these cases, no variations of the position of the OLTC are forced.
- $\delta\varepsilon > 0$, if only the upper voltages constraints are violated ($\varepsilon_2 > 0$) or $\varepsilon_2 > \varepsilon_1$. In this cases, the position of the tap selector is modified to reduce the voltage at the busbar (node N02 in Fig. 2), and along the feeders.
- $\delta\varepsilon < 0$, if only the lower voltages constraints are violated ($\varepsilon_1 > 0$) or $\varepsilon_1 > \varepsilon_2$. In this case, the position of the tap selector is modified to increase the voltage at the busbar (node N02 in Fig. 2).

In any case, and in order to avoid high frequency switching, the previous conditions must be maintained for a prescribed "dwell time" T_s before the tap position is allowed to switch for the first time or after a previous commutation.
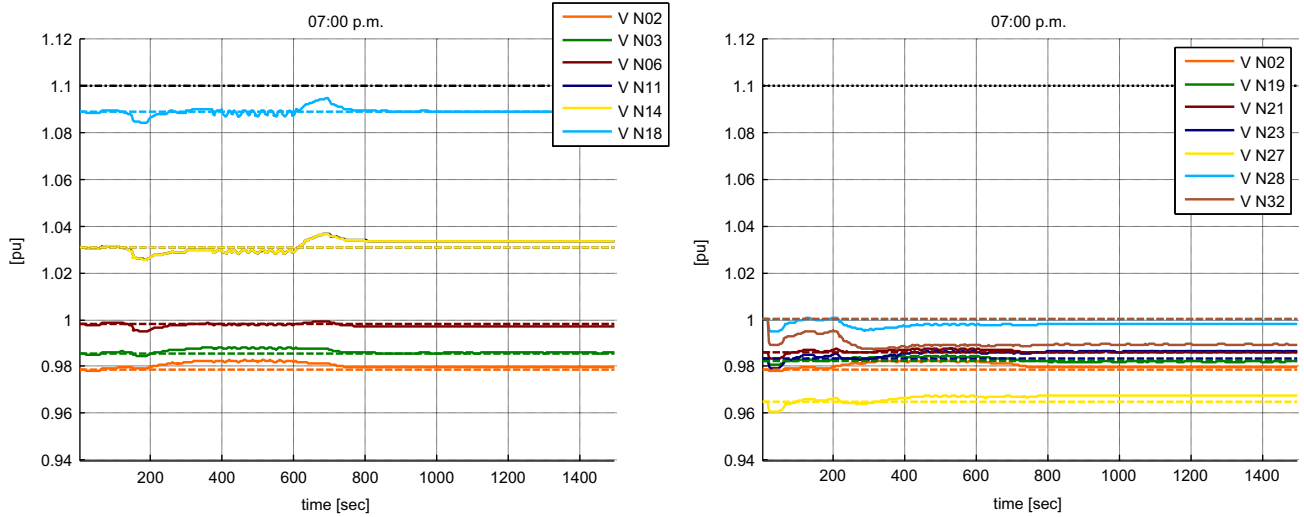
Fig. 8. Experiment 1–7 p.m. voltages at the nodes of the first (left) and second (right) feeder. Dashed lines: reference values. Dash-dotted black line: $1+Y_{max}$.
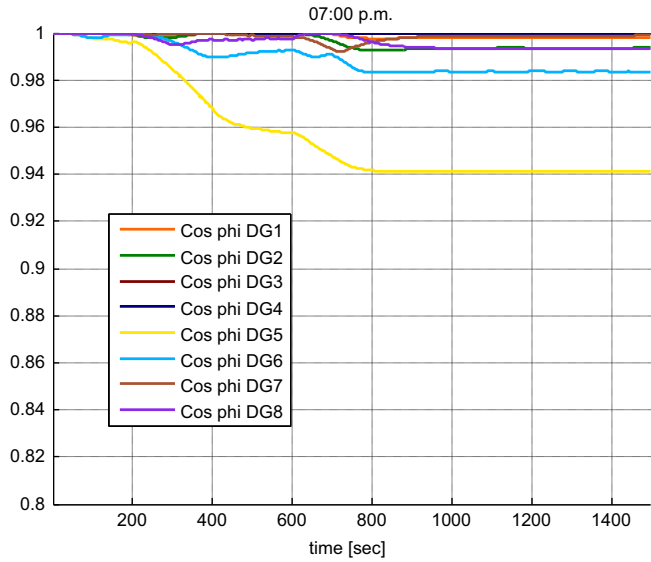

Fig. 9. Experiment 1–7 p.m. reference power factors computed by the MPC algorithm.

3. Case study

3.1. Description of the benchmark network

The case study, depicted in Fig. 2, consists of a rural radial MV (20 kV), made by two feeders, eight DGs (photovoltaic, aeolian, turbogas), and thirty-one loads (industrial, agricultural, residential, tertiary, public lighting). For simplicity, all the DGs have been modeled as fifth order synchronous generators in the Park trans-formation domain. Feeder 1 is 27 km long with seventeen nodes and five DGs, while Feeder 2 is 36.9 km long with fourteen nodes and three DGs. A number of working points, corresponding to the load and generation profiles at hours 1 a.m., 7 a.m., 1 p.m., 7 p.m. of the day have been considered. The main characteristics of the DGs, of the loads in these working points, and of the network elements are reported in the Appendix A. Note that the considered operating conditions are significantly different from each other in terms of power production of the DGs and of the loads.

A detailed simulator of the network, used both in the identification and for validating and testing the performance of the overall control scheme, has been developed in the DIgSILENT environment.

3.2. Identification of the impulse-response model and MPC design

For identification purposes, once the local PI regulators of the generators have been properly tuned using empirical rules, the DIgSILENT reference simulator described in the previous section has been used to generate open loop step response output signals. Specifically, in a single test, every 30 s, a step variation has been imposed to each input and each disturbance signal, as detailed in Table 1. From the elements of the step response, the coefficients of the impulse response are readily computed by differentiation.

Note that:

- The nominal identification conditions for the model are those corresponding to the state of the network at 7 a.m.
- The output (controlled) variables are eleven voltages, five corresponding to nodes N03, N06, N11, N14, N18 (see Fig. 2) of feeder 1 and six corresponding to nodes N19, N21, N23, N27, N28, N32 of feeder 2. The input manipulated variables are the reference values of the internal loops of the reactive power factors of the eight distributed generators. Finally, the active powers of the distributed generators DG1, DG2, and DG3 have been considered as known disturbances, while the powers produced by the other DGs and all the loads have been assumed to be unknown disturbances.
- The sampling time of the identified impulse-response model has been set to $T = 2$ s.
- Since we estimate that the impulse response is practically exhausted after 90 sampling times, we set $M = 90$ regressors.

The plots corresponding to the identification tests are not shown here for brevity. The model validation is implicitly performed through the closed-loop simulation experiments described in Sections 3.4, 3.5 and 3.6.

3.3. The simulation environment and control tuning

A DIgSILENT simulator plays the role of the controlled plant in the experiments described in the following. Indeed, the physical grid, including generators and their dynamic models, have been implemented in DIgSILENT, as well as local regulators (active power and power factor regulators). DIgSILENT PowerFactory is a well proven, industry-standard power system simulator, able to model and analyze transmission and distribution grids with various components.
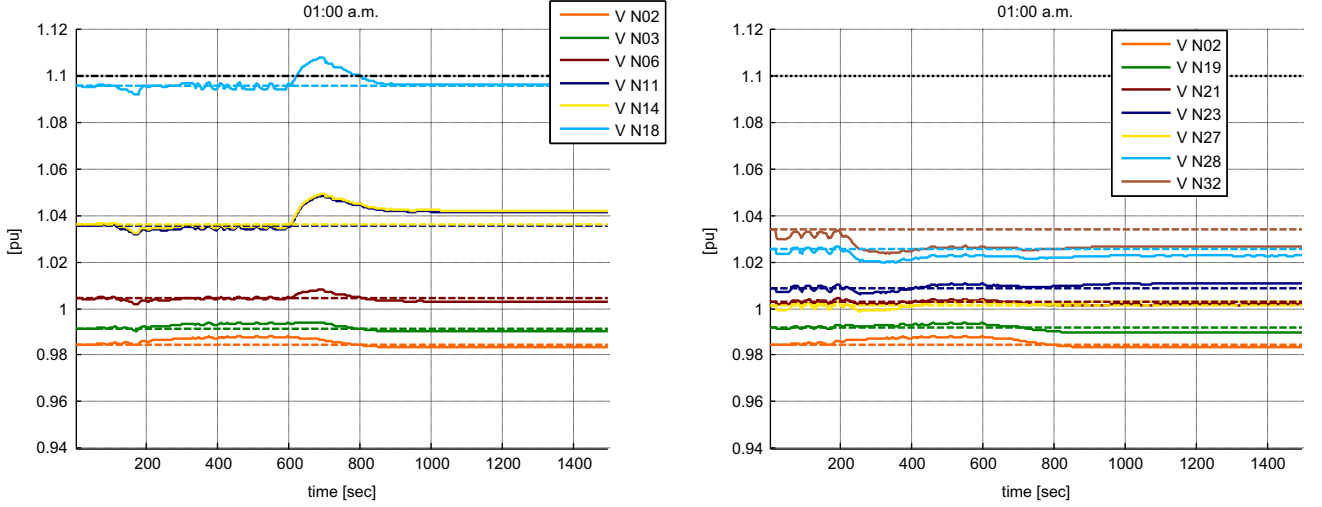
Fig. 10. Experiment 1–1 a.m. voltages at the nodes of the first (left) and second (right) feeder. Dashed lines: reference values. Dash-dotted black line: $1+Y_{max}$.
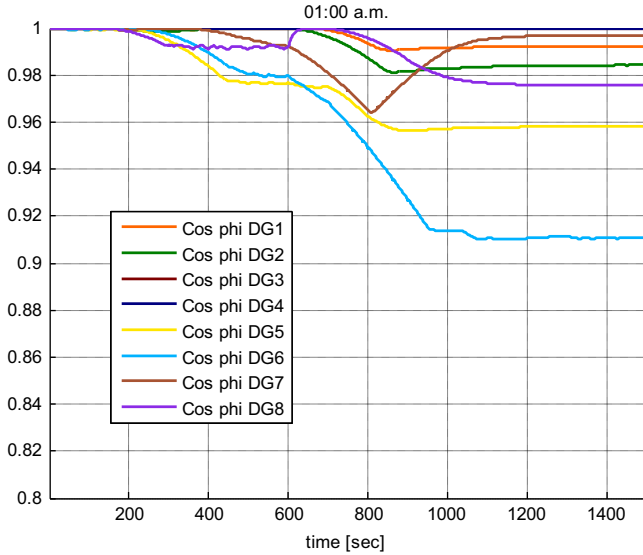

Fig. 11. Experiment 1–1 a.m. reference power factors computed by the MPC algorithm.

However, due to the difficulties of coding optimization-based control algorithms in DIgSILENT, the MPC controller has been imple-mented in MATLAB and an ad hoc software interface, called DGS-SimLab (see Fig. 3), has been developed to link and synchronize the MATLAB environment with DIgSILENT. The core of DGS-SimLab lies in a custom DLL Interface file, which contains proper functions, which are periodically run by DIgSILENT. These functions (i) pause the DIgSILENT simulation; (ii) write the required measurements and a timestamp in a file in the Data Exchange System; (iii) perform a call of the MPC control algorithm; (iv) load the new control inputs, computed by the MPC algorithm, as soon as they get written – by the MATLAB control function – in the Data Exchange System; (v) resume the simulation.

The prediction horizon $N=10$ has been selected, while only two variations of the future control variables have been allowed, i.e. $N_u=2$. The weighting matrices have been set as $Q=10I$, $R=0.1I$, where I is the identity matrix of appropriate dimensions. Moreover, it has been set $\mu_1=\mu_2=1000$. The absolute controlled voltages (in per units) have been constrained to belong to the interval [0.9, 1.1] p.u.,

while the reference power factors have been constrained to belong to the interval [0.6,1]. Consistently, concerning the output and input variables $y(k)$ and $u(k)$, they are bound to lie in the intervals $[-0.1,0.1]$ and $[-0.4,0]$, respectively.

3.4. Experiment 1

The performances of the MPC regulator, based on the impulse response model computed at 7 a.m., have been tested in the four operating conditions specified in the Appendix A. Specifically, the perturbations listed in Table 2 have been given to some DGs and loads; note that their size is significantly large compared to the corresponding nominal values.

First, the network has been considered to be in the nominal stationary operating conditions at 7 a.m., which however does not correspond to the desired equilibrium due to a too high voltage at node N18. Therefore, the regulator has the twofold objective to reach the required nominal operating point and to counteract the variations of Table 2. The transients of the absolute values of the voltages at the controlled nodes are reported in Fig. 4, and show the excellent behavior of the controlled system: the upper and lower voltage constraints, i.e. [0.9, 1.1] p.u., are satisfied (save for an initial transient due to the initial operating conditions outside these boundaries), and the voltages tend to reach the correspond-ing steady-state values. The controlled reference power factors of the DGs are shown in Fig. 5.

The ability of the MPC regulator, based on the model at 7 a.m., to control the DIgSILENT simulator of the network at different operat-ing conditions has been tested starting from the nominal conditions at 1 a.m, 1 p.m. and 7 p.m. and applying the same power variations summarized in Table 2. The obtained voltage profiles are reported in the following Figs. 6, 8, and 10. Fig. 7, 9, and 11 depict the corresponding reference power factors of the DGs. These results show a slight deterioration of the performances due to the presence of an oscillatory behavior in many transients. However, the size of these oscillations is small, and could easily be smoothed with a simple filtering action on the implemented power factors. This has not been done here to fairly evaluate the performances of the control algorithm at operating conditions very different from those at 7 a.m., where the network impulse response model has been derived. Note however that the voltage constraints are always met, save for the transient of N18 at 1 a.m. (see Fig. 10, left panel), when no feasible solution exists for the stated optimization problem and
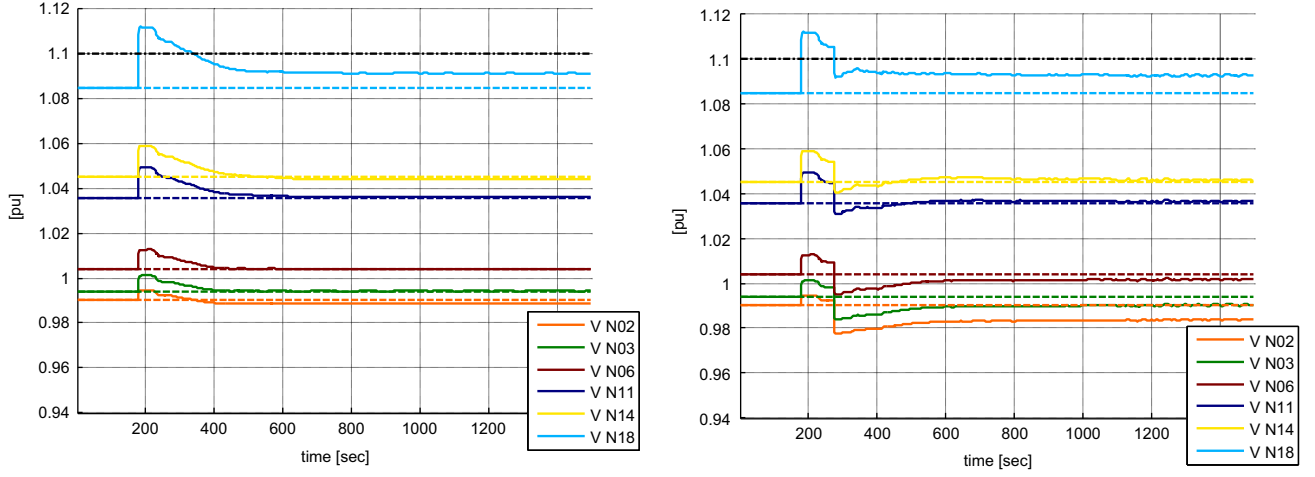
Fig. 12. Experiment 2 – voltages at the nodes of the first feeder. Left: without OLTC control, right: with OLTC control. Dash-dotted black line: $1+Y_{max}$.
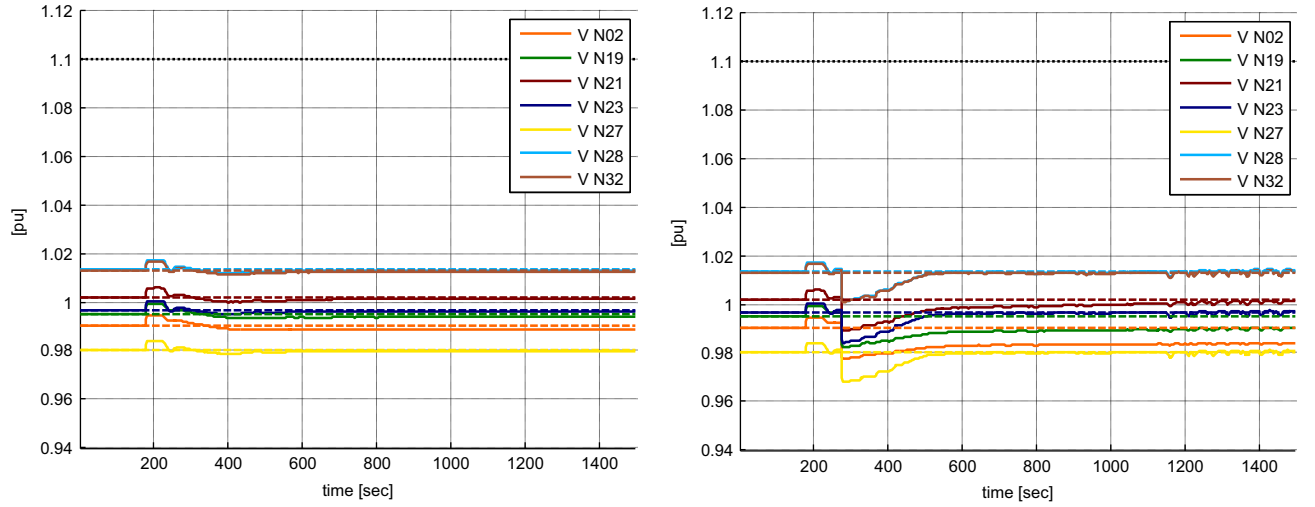
Fig. 13. Experiment 2 – voltages at the nodes of the second feeder. Left: without OLTC control, right: with OLTC control. Dash-dotted black line: $1+Y_{max}$.

the corresponding slack variable takes values different from zero. In order to improve this, it could be possible to adapt the MPC algorithm to varying operating conditions, as discussed in the final section of the paper.

3.5. Experiment 2

Considering again the conditions at 7 a.m., a simulation has been performed by disconnecting at time $t=180$ s the loads at nodes N03 and N18, both belonging to the first feeder. The transients of the controlled voltages with and without the OLTC controller, are compared in Figs. 12 and 13. In the implementation of the OLTC controller, a dwell time $T_s=75$ s has been used. It is apparent that the critical voltage at node N18 (see Fig. 12) returns within the prescribed limits much faster when the OLTC action becomes available.

3.6. Experiment 3

In this section we show the results of the performance comparison between the MPC technique proposed in the paper and a traditional control system denoted *coordinated control*. The

Fig. 14. Experiment 3 – active power of the DGs.

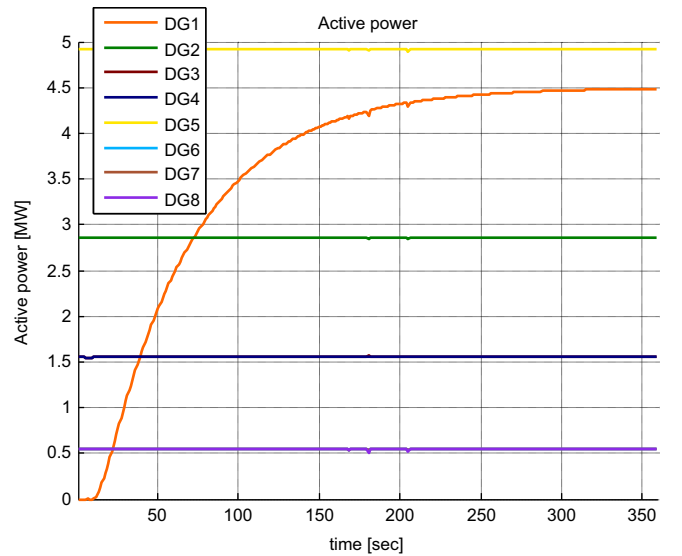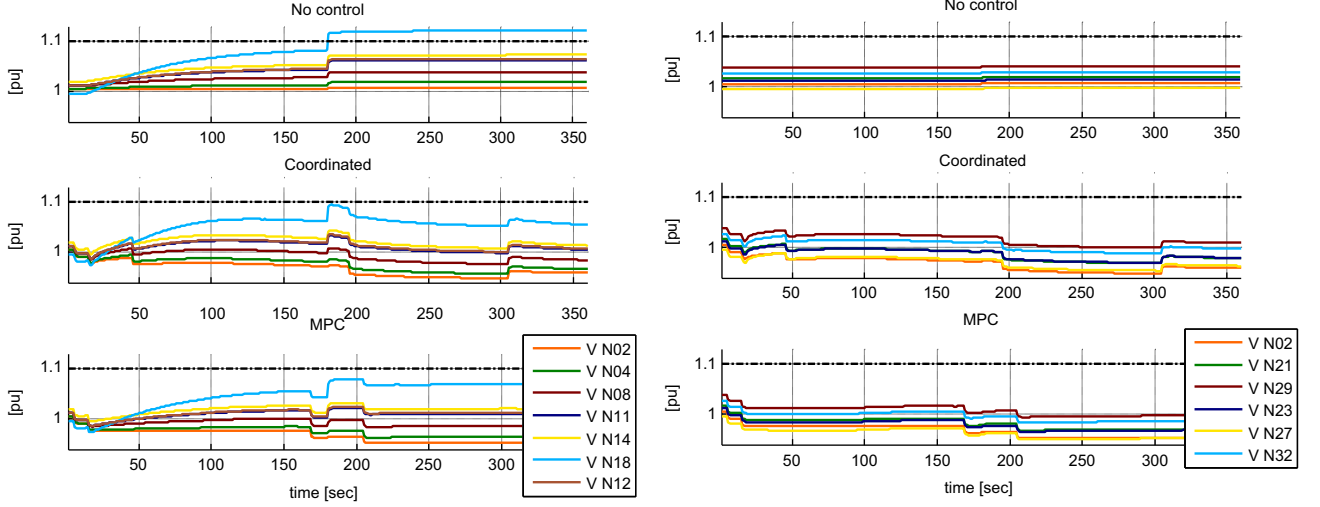**Fig. 15.** Experiment 3 – voltages at the nodes of the first (left) and second (right) feeder for three cases: no control (up), coordinated control (middle), MPC (down). Dash-dotted black line: $1 + Y_{max}$.
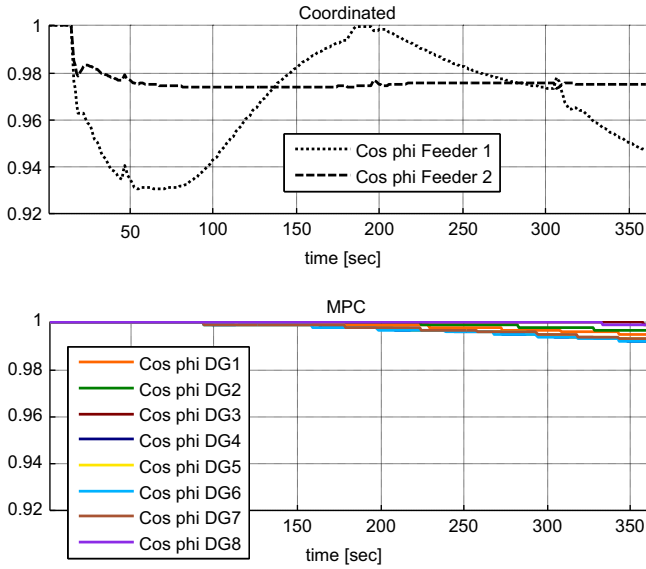

Fig. 16. Experiment 3 – reference power factors for the DGs: coordinated control (up), MPC (down).

coordinated control system is a PI-based regulator with the objective of controlling both the OLTC and the feeders. Concerning the latter, each feeder is endowed of an independent controller, which computes a unique power factor set-point of the feeder's distributed generators with the aim of attaining a reactive power reference Q_{rif} at the beginning of the feeder. On the other hand, the OLTC controller has the objective of regulating the voltage at the tap changer level at a reference set-point V_{rif}, computed as the sum of the nominal reference voltage and of additive voltage and current compensation terms. For more details please see (Corsetti, Guagliardi, & Sandroni 2014).

Considering the conditions at 7 a.m., a simulation has been performed by considering the following case: at time $t = 0$ all DGs are on but DG1, which starts producing power (until about 4.5 MW in steady state), as depicted in Fig. 14. At time $t = 180$ s three loads get switched off: C16, C17 e C18, located on the first feeder near DG1. The total amount of load loss is about 1.4 MW.

The transients of the controlled voltages are compared in Fig. 15, where three scenarios are simulated: the case where no

control action is done, the case where the coordinated control is used, and the case where MPC is implemented. In Fig. 16 we depict the reference power factors for the distributed generators in case of coordinated control and MPC (note that the coordinated controller fixes a unique reference power factor for all the DGs of each feeder). We can conclude that, while both control systems are able to prevent excessive voltages, the proposed MPC scheme minimizes the single generators' power losses in view of the fact that the power factors are maximized.

With the available tools (i.e., HW: Intel i5-2400@3.1 GHz (quadcore), 4 GB; SW: Win7 64 bit operating system, DIgSILENT PowerFactory 14.1, Matlab 2014a) and with the described tuning of the MPC algorithm, we could perform accelerated simulations with respect to the adopted sampling time. Indeed for simulating the case study (simulation time: 60 min) the computational times are the following. No control: 28 s, coordinated control: 30 s, MPC: 45 s.

4. Conclusions

The MPC algorithm proposed in this paper has been proved to be effective to control a complex benchmark describing a MV rural network working at the different operating conditions. This network represents a challenging test case, which calls for the solution of a large scale and multivariable control problem, with more controlled variables than manipulated inputs, and with more disturbances than manipulated variables. In addition, a physical model of the system would result to be too complex for the control design and stringent constraints must be met to cope with realistic conditions.

The proposed mixed control strategy, combining both the use of the OLTC and the participation of the DGs, led satisfactory results which can be further improved in many ways, for example by adopting some kind of adaptation mechanism. This can be done by simply modifying the weighting matrices appearing in the cost function at any new operating point according to a gain scheduling procedure. In addition, one could also rely on different linearized (impulse response) models determined at any new operating condition by means of the more complex and reliable simulator developed in DIgSilent.

Further extensions of the proposed control scheme will deal with distributed implementations of the controller, see (Scattolini, 2009) for a survey of available distributed MPC methods, or on the use of a larger number of slack variables, one for each voltage constraint, to refine the control logic governing the OLTC.

Appendix A

See Tables 3–9.

Table 3
Distributed generators (PV: photovoltaic, TG: turbogas, AE: Eolic).

DG	Feeder	P [MW] Nominal	P [MW] 1 a.m.	P [MW] 7 a.m.	P [MW] 1 p.m.	P [MW] 7 p.m.
DG1 - TG	1	5.5	4.95831	4.922	4.949614	4.964138
DG2 - TG	1	3.2	2.884827	2.864	2.879755	2.88806
DG3 - PV	1	3.2	0	1.559	2.056134	0
DG4 - PV	2	3.2	0	1.559	2.056124	0
DG5 - TG	2	5.5	4.958303	4.923	4.949595	4.963955
DG6 - AE	2	5.5	0.748335	0.549	3.245381	1.495977
DG7 - AE	1	5.5	0.823168	0.549	3.569903	1.645546
DG8 - AE	1	5.5	0.823169	0.549	3.569924	1.645603

Table 4
HV/MV transformers.

Model	40 MVA132/20
Rated power	50 MVA
Copper losses	176 kW
Relative short-circuit voltage	15.5%
Number of taps	12 (+6 … −6)
Voltage per tap	1.5%

Table 5
MV/LV transformers.

Model	0.25 MVA 20 kV/0.4	0.4 MVA 20 kV/0.4	0.63 MVA 20 kV/0.4
Rated power	250 kVA	400 kVA	630 kVA
Copper losses	2.6 kW	3.7 kW	5.6 kW
Relative short-circuit voltage	4%	4%	6%
Number of transformers	6	7	5

Table 6
Transformers.

Name	Type
TR AT/MT	40 MVA132/20
TR1.05	0.63 MVA 20 kV/0.4
TR1.07	0.4 MVA 20 kV/0.4
TR1.09	0.25 MVA 20 kV/0.4
TR1.11	0.25 MVA 20 kV/0.4
TR1.13	0.25 MVA 20 kV/0.4
TR1.14	0.25 MVA 20 kV/0.4
TR1.15	0.25 MVA 20 kV/0.4
TR2.19	0.63 MVA 20 kV/0.4
TR2.20	0.4 MVA 20 kV/0.4
TR2.21	0.4 MVA 20 kV/0.4
TR2.24	0.4 MVA 20 kV/0.4
TR2.25	0.4 MVA 20 kV/0.4
TR2.27.1	0.63 MVA 20 kV/0.4
TR2.27.3	0.63 MVA 20 kV/0.4
TR2.28	0.25 MVA 20 kV/0.4
TR2.30	0.63 MVA 20 kV/0.4
TR2.31	0.4 MVA 20 kV/0.4
TR2.32	0.4 MVA 20 kV/0.4

Table 7
Lines.

Name	Type	Section [mm^2]	R [Ω/km]	L [mH/km]	C [μF/km]
ARG7H1RX 120 mmq	Cable	120	0.3330	0.382	0.2500
ARG7H1RX 185 mmq	Cable	185	0.2180	0.350	0.2900
ARG7H1RX 70 mmq	Cable	70	0.5800	0.414	0.2100
Aerea Cu 25 mmq	Overhead	25	0.7200	1.389	0.0083
Aerea Cu 70 mmq	Overhead	70	0.2681	1.286	0.0090

Table 8
Lines characteristics.

Name	Type	Length [km]	Feeder
D1-02_03	ARG7H1RX 185 mmq	1.884	1
D1-03_04	ARG7H1RX 185 mmq	1.62	1
D1-04_05	ARG7H1RX 185 mmq	0.532	1
D1-05_06	ARG7H1RX 185 mmq	1.284	1
D1-06_07	ARG7H1RX 120 mmq	1.618	1
D1-07_08	ARG7H1RX 120 mmq	0.532	1
D1-08_09	ARG7H1RX 185 mmq	2	1
D1-09_10	ARG7H1RX 185 mmq	2.4	1
D1-10_11	ARG7H1RX 120 mmq	2.252	1
D1-11_12	ARG7H1RX 185 mmq	0.756	1
D1-12_13	Aerea Cu 25 mmq	1.87	1
D1-12_15	ARG7H1RX 120 mmq	1.19	1
D1-13_14	Aerea Cu 25 mmq	1.28	1
D1-15_16	ARG7H1RX 120 mmq	0.8	1
D1-16_17	Aerea Cu 25 mmq	3	1
D1-17_18	Aerea Cu 25 mmq	4	1
D2-02_19	ARG7H1RX 185 mmq	3.6	2
D2-19_20	ARG7H1RX 185 mmq	3.304	2
D2-20_21	Aerea Cu 70 mmq	2.4	2
D2-21_22	Aerea Cu 70 mmq	3.6	2
D2-22_23	Aerea Cu 70 mmq	3	2
D2-22_28	ARG7H1RX 70 mmq	2.4	2
D2-23_24	Aerea Cu 70 mmq	3.08	2
D2-24_25	Aerea Cu 70 mmq	1.65	2
D2-25_26	Aerea Cu 70 mmq	1.8	2
D2-26_27	Aerea Cu 70 mmq	2.2	2
D2-28_29	ARG7H1RX 70 mmq	2.2	2
D2-29_30	ARG7H1RX 70 mmq	2.4	2
D2-30_31	ARG7H1RX 70 mmq	2.6	2
D2-31_32	ARG7H1RX 70 mmq	2.7	2

Table 9

Loads – type: A=Agricultural, R= residential, T=tertiary, I=industrial, L=public lighting, LV=low voltage, MV=medium voltage.

LOAD	Type	P [MW] 1 a.m.	Q [MVAR] 1 a.m.	P [MW] 7 a.m.	Q [MVAR] 7 a.m.	P [MW] 1 p.m.	Q [MVAR] 1 p.m.	P [MW] 7 p.m.	Q [MVAR] 7 p.m.
N03	I-MV	0.4241	0.2056382	1.7007	0.8274	1.5251	0.7443214	0.512171	0.2506077
N04	T-MV	0.0880	0.0435790	0.2206	0.1098	0.3982	0.2027317	0.398178	0.2021694
N05	R-LV	0.1266	0.0849696	0.0919	0.0619	0.1865	0.1258367	0.223849	0.1504288
N06	I-MV	0.2987	0.1466945	1.1963	0.5878	1.0766	0.534423	0.360688	0.178627
N07	R-LV	0.0742	0.0505676	0.0537	0.0367	0.1101	0.0758206	0.131505	0.0899172
N08	T-MV	0.0806	0.0421746	0.2018	0.1056	0.3667	0.20039	0.364454	0.1949992
N09	T-LV	0.0224	0.0163072	0.0558	0.0401	0.1011	0.0749315	0.100247	0.07218664
N10	I-MV	0.0690	0.0346640	0.2764	0.1388	0.2502	0.1283052	0.083363	0.04221028
N11	L-LV	0.0848	0.0556931	0	0	0	0	0.069140	0.04507657
N13	R-LV	0.0669	0.0463782	0.0488	0.0341	0.1016	0.0722708	0.118290	0.0821189
N14	R-LV	0.0608	0.0422226	0.0446	0.0313	0.0929	0.0664264	0.107698	0.07484372
N15	T-LV	0.0183	0.0140455	0.0455	0.0346	0.0831	0.0671084	0.081832	0.06273277
N16	I-MV	0.1196	0.0609686	0.4786	0.2438	0.4341	0.2269448	0.144368	0.07421394
N17	R-MV	0.2124	0.1096805	0.1525	0.0785	0.3193	0.1679388	0.378381	0.1965451
N18	I-MV	0.2115	0.1131246	0.8431	0.4468	0.7641	0.414908	0.255114	0.1372592
N19	I-LV	0.0528	0.0354222	0.2109	0.1401	0.1894	0.1265088	0.063739	0.04289173
N20	A-LV	0.0570	0.0383210	0.1533	0.1028	0.1147	0.0774413	0.153274	0.1027773
N21	A-LV	0.0572	0.0385852	0.1536	0.1032	0.1155	0.0782289	0.153287	0.1027909
N23	L-MV	0.2321	0.1110559	0	0	0	0	0.182994	0.08827465
N24	A-LV	0.0543	0.0366918	0.1439	0.0961	0.1094	0.0741473	0.143659	0.0958174
N25	I-LV	0.0404	0.0274218	0.1598	0.1054	0.1450	0.0984401	0.048166	0.03204506
N26	T-MV	0.0883	0.0442469	0.2174	0.1033	0.3993	0.2049369	0.388592	0.1829258
N27	R-LV	0.1685	0.1128906	0.1193	0.0787	0.2471	0.1656134	0.285200	0.1853766
N27.2	A-MV	0.3021	0.1470421	0.8023	0.3866	0.6083	0.2971269	0.799597	0.384729
N27.3	A-LV	0.1048	0.0704947	0.2744	0.1814	0.2094	0.1407233	0.273508	0.1805081
N28	T-LV	0.0270	0.0197459	0.0664	0.0464	0.1205	0.08741	0.118186	0.08054955
N29	I-MV	0.0434	0.0220095	0.1726	0.0864	0.1561	0.0798601	0.051826	0.02596448
N30	I-LV	0.0541	0.0378280	0.2135	0.1453	0.1934	0.1347733	0.064483	0.04441056
N31	A-LV	0.0467	0.0319818	0.1234	0.0835	0.0934	0.0640347	0.123344	0.08350521
N32.1	R-LV	0.0910	0.0630751	0.0643	0.0439	0.1333	0.0923274	0.155504	0.1052517
N32.2	A-MV	0.2807	0.1388702	0.7457	0.3652	0.5634	0.2791258	0.745457	0.3650585

References

Aquino-Lugo, A., Klump, R., & Overbye, T. J. (2011). A control framework for the smart grid for voltage support using agent-based technologies. *IEEE Transactions on Smart Grid*, *2*(1), 173–180.

Biserica, M., Bersaneff, B., Besanger, Y., & Kieny, C. (2011). Upgraded coordinated voltage control for distribution systems. *PowerTech*, 1–6.

Camacho, E., & Bordons, C. (2007). *Model predictive control*. Springer.

Corsetti, E., Guagliardi G. A., Sandroni C. Strategie per il controllo di reti di distribuzione attive in MT e di microgrid in BT, Rapporto di Ricerca di Sistema 14000645, RSE, 2014, (in Italian), (in press).

Gao, C., Redfern, M. A. A review of voltage control techniques of networks with distributed generations using on-load tap changer transformers. In *Proceedings of the 45th International Conference of Universities Power Engineering Conference (UPEC)*, 2010 , 2010.

Grüne, L., Rantzer, A. On the infinite horizon performance of receding horizon controllers, *IEEE Transactions on Automatic Control*, *53* (9), 2100–2111.

Hojo, M., Hatano, H., Fuwa, Y. Voltage rise suppression by reactive power control with cooperating photovoltaic generation systems, In *Proceedings of the 20th Conference on CIRED* 2009, paper No. 301, Prague, 2009.

Huneault, M., & Galiana, F. D. (1991). A survey of the optimal power flow literature. *IEEE Transactions on Power Systems*, *6*(2), 762–770.

Jadbabaie, A., Hauser, J. On the stability of receding horizon control with a general terminal cost, *IEEE Transactions on Automatic Control*, *50* (5), 674–678,2005.

Kiprakis, A. E., Wallace, A. R. Hybrid control of distributed generators connected to weak rural networks to mitigate voltage variation. In *Proceedings of the CIRED* 2003, paper No. 44, Barcelona, 2003.

Liu, X., Aichhorn, A., Liu, L., & Li, H. (2012). Coordinated control of distributed energy storage system with tap changer transformers for voltage rise mitigation under high photovoltaic penetration. *IEEE Transactions on Smart Grid*, *3*(2), 897–906.

Mayne, D. Q., Rawlings, J. B., Rao, C. V., & Scokaert, P. O. M. (2000). Constrained model predictive control: stability and optimality. *Automatica*, *36*(6), 789–814.

Petrone F., Farina, M., Guagliardi, G., Sandroni, C., Scattolini, R., Veneroni, A. Object-oriented modeling of a power network for model-based voltage control. In *Proceedings of the CIRED 2012 Workshop*, paper No. 258, Lisbon, 2012. Richardot O., Viciu, A., Besanger, Y., Kieny C. Coordinated voltage control in distribution networks using distributed generation. pp. 1196–1201. In *Proceedings of the Transmission and Distribution Conference and Exhibition, PES*, 2006.

Scattolini, R. (2009). Architectures for distributed and hierarchical model predictive control – a review. *Journal of Process Control*, *19*, 723–731.

Turitsyn, K., Šulc, P., Backhaus, S, & Chertkov, M. (2011). Options for control of reactive power for distributed photovoltaic generators. *In Proceedings of the IEEE*, *99*(6), 1063–1073.

Valverde, G., & Van Cutsem, T. (2013). Model predictive control of voltages in active distribution networks, *IEEE Transactions on Smart Grids*, *4*(4), 2152–2161. Viawan, F.A., Karlsson, D. Coordinated voltage and reactive power control in the presence of distributed generation. In *Proceedings of the Power and Energy Society General Meeting – Conversion and Delivery of Electrical Energy in the 21st Century, IEEE*, 2008.

Vovos, P. N., Kiprakis, A. E., Wallace, A. R., & Harrison, G. P. (2007). Centralized and distributed voltage control: impact on distributed generation penetration. *IEEE Transactions on Power Systems*, *22*, 476–483.

Xu T., Taylor P. C. Voltage controltechniques for electrical distribution networks including distributed generation. In *Proceedings of the 17th IFAC World Congress*, (pp. 11967–11971), Seoul, Korea, 2008.

Yu, L., Czarkowski, D., & de Leon, F. (2012). Optimal distributed voltage regulation for secondary networks with DGs. *IEEE Transactions on Smart Grid*, *3*(2), 959–967.